Available online at www.sciencedirect.com

ScienceDirect

Physics Procedia 00 (2009) 000–000

Physics Procedia

www.elsevier.com/locate/procedia

14th International Conference on Narrow Gap Semiconductors and Systems

Rectangular model of a ballistic spin interferometer in (001) InGaAs/InAlAs quantum wells

Takaaki Koga[a,b,c,*,**], S. Faniel[a,**], S. Mineshige[b], T. Mastuura[c,**] and Y. Sekine[d]

[a]*Graduate School of Information Science and Technology, Hokkaido University, Sapporo, Hokkaido, 060-0814, Japan*
[b]*Faculty of Engineering, Hokkaido University, Sapporo, Hokkaido, 060-8628, Japan*
[c]*Creative Research Institution Sousei Research Department, Hokkaido University, Sapporo, Hokkaido, 001-0021, Japan*
[d]*NTT Basic Research Laboratories, NTT Corporation, Atsugi, Kanagawa, 243-0198, Japan*

Elsevier use only: Received date here; revised date here; accepted date here

Abstract

We report an unambiguous detection of the crytalline anisotropy of the spin-orbit interaction in (001) InAlAs/InGaAs/InAlAs quantum wells using nanofabricated rectangular loop arrays, where the sides of the constituent loops are aligned along either the [110] or [1$\bar{1}$0] crystallographic axis. The fabrication and measurements were performed on the epi-wafer samples whose spin properties were characterized previously [Koga *et al.*, Phys. Rev. Lett **89**, 046801 (2002)]. We find that the experimentally observed spin interference patterns — the amplitude modulation of the Al'tshuler-Aronov-Spivak oscillations as a function of the gate voltage — are in good agreement with the results of the spin interferometer model extended for rectangular loops and including both the Rashba and Dresselhaus spin-orbit interactions.
PACS: **71.28.+d**; 71.70.Ej; **72.25.-b**; 72.25.Dc; 72.25.Rb; 72.80.Ey; 73.20.Fz; 73.21.Fg; **73.23.-b**; 73.23.Ad;

Keywords: spintronics; spin interference; Rashba effect; Dresselhaus effect; spin-orbit interaction; quantum wells; mesoscopic transport

1. Introduction

There has been much interest in the control of electron spin dynamics, through the control of the Rashba and Dresselhaus spin-orbit (S.O.) interactions in III-V semiconductor heterostructures. In this paper, we extend our previous model of ballistic spin interferometer (SI) based on the Rashba effect [1,2], to the one that includes both the Rashba and Dresselhaus S.O. interactions in more general rectangular loop geometries. We itemize the underlying assumptions and conditions as follows: (1) The interferometer (nanolithographically defined rectangular loop arrays) is fabricated in *n*-type (001) $In_{0.52}Al_{0.48}As/In_{0.53}Ga_{0.47}As/In_{0.52}Al_{0.48}As$ quantum wells (QW), where the direction of [001] axis ($\hat{z}$ direction) is defined to be pointing upward from the semiconductor surface. (2) The Rashba parameter α [see Eq.(3)] has the same sign as the z component of the electric field (E_z) within the QW

* Corresponding author. Tel.: +81-11-706-6538; fax: +81-11-706-7803.
E-mail address: koga@ist.hokudai.ac.jp.
** This work is supported by KAKENHI, Grant-in-Aid for Young Scientists (A), No. 19684009. Grant-in-Aid for JSPS fellow, financial support from Iketani Science and Technology Foundation and Grants-in-Aid from Hokkaido Innovation through Nanotechnology Support (HINTS) are also highly acknowledged.

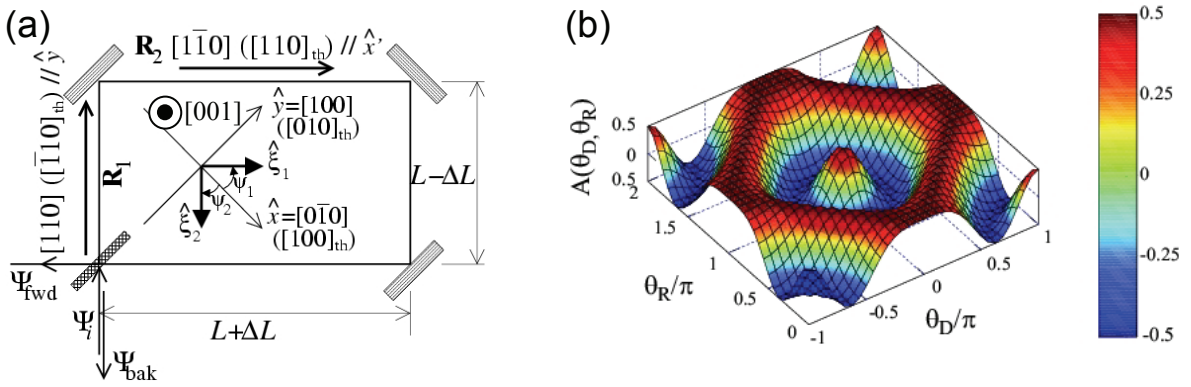

Fig.1. (a) Illustration of a rectangular spin interferometer. Placed at the lower left corner is a hypothetical beam splitter. Placed at the other three corners are totally reflective mirrors. (b) Three dimensional plot of $A(\theta_D, \theta_R)$ [Eq. (6)].

(pointing in the [001] direction), according to the **k**·**p** theory, assuming that the contributions from the hetero-interface boundaries [3] are negligible. (3) The sides of the rectangular loops are aligned along either the [110] (vertical) or the [1$\bar{1}$0] (horizontal) crystallographic axes.

A noteworthy result in the analysis of our experimental work is the detection of the crystallographic anisotropy of the S.O. interaction. We prepared two kinds of rectangular loop samples. In one kind, the constituent rectangles were elongated horizontally (|| [1$\bar{1}$0]), denoted by positive values of ΔL. In the other kind of samples, the rectangles were elongated vertically (|| [110]), denoted by negative values of ΔL [see Fig. 1(a)]. We observed distinct spin interference (SI) patterns, which are also denoted as the time-reversal Aharonov-Casher (TRAC) patterns [4], between these two kinds of samples, where the peak and dip features of the SI patterns were consistent with our extended SI model.

2. Spin Interferometer Model

Shown in Fig. 1(a) is a schematic illustration of the rectangular SI. We consider the evolution of the spin state Ψ_i that is incident at the lower left corner of the loop in both the clockwise (CW) and counter-clockwise (CCW) directions [only the clockwise direction is shown in Fig. 1(a)]. The transport electron experiences spin precession due to the Rashba and Dresselhaus S.O. interactions. We denote the spin states of an electron after propagating the loop in the CW and CCW directions, respectively, as Ψ_{CW} and Ψ_{CCW}.

$$\Psi_{\mathrm{CW}} = e^{-i\frac{\phi}{2}}\mathbf{R}_4\mathbf{R}_3\mathbf{R}_2\mathbf{R}_1\Psi_i \equiv e^{-i\frac{\phi}{2}}\mathbf{R}_{\mathrm{TOT}}\Psi_i \ \text{ and } \ \Psi_{\mathrm{CCW}} = e^{i\frac{\phi}{2}}\mathbf{R}_1^{-1}\mathbf{R}_2^{-1}\mathbf{R}_3^{-1}\mathbf{R}_4^{-1}\Psi_i \equiv e^{i\frac{\phi}{2}}\mathbf{R}_{\mathrm{TOT}}^{-1}\Psi_i. \quad (1)$$

where $e^{\pm i\frac{\phi}{2}}$ is the phase added to account for the magnetic flux piercing the loop ($\phi = 2\pi\Phi\Phi_0^{-1} = 2\pi BS\left(\frac{h}{e}\right)^{-1}$, S being the area inside the loop). $\mathbf{R}_1$~$\mathbf{R}_4$ are the spin rotation operators associated with the electron transport along each side of the loop. We note that $\mathbf{R}_4=\mathbf{R}_2^{-1}$ and $\mathbf{R}_3=\mathbf{R}_1^{-1}$ by the time-reversal symmetry. We also assume that Ψ_i is properly normalized. The backscattering portion of the partial wave function is written as $\Psi_{bak}=1/2(\Psi_{CW}+\Psi_{CCW})$. The factor 1/2 is obtained by multiplying $1/\sqrt{2}$ twice, each $1/\sqrt{2}$ being associated with the beam splitter [1]. We relate $|\Psi_{bak}|^2$ to the quantum correction to the electric resistance (R_{xx}). The larger $|\Psi_{bak}|^2$, the larger R_{xx}. Since Ψ_i can take all spin states with equal probabilities, the averaged value of $|\Psi_{bak}|^2$ over all initial spin states, denoted by $\overline{|\Psi_{bak}|^2}$, is the measure of the quantum correction to R_{xx}. With a little algebra, one can show

$$\overline{|\Psi_{\mathrm{bak}}|^2} = \frac{1}{2} + \left\{ \left(\frac{[\mathbf{R}_{\mathrm{TOT}}]_{\uparrow\uparrow} + [\mathbf{R}_{\mathrm{TOT}}]_{\downarrow\downarrow}}{2} \right)^2 - \frac{1}{2} \right\} \cos\phi \equiv \frac{1}{2} + A\cos\phi, \quad (2)$$

where $[\mathbf{X}]_{\sigma\sigma'}$ denotes a matrix element $\langle\sigma|\mathbf{X}|\sigma'\rangle$ ($\sigma, \sigma' = \uparrow$ or $\downarrow$) using a spin basis in $\hat{z}$ direction. $\mathbf{R}_{\mathrm{TOT}}$ is given in Eq. (1) and the detailed forms for $\mathbf{R}_1$~$\mathbf{R}_4$ are discussed below. We note that $\cos\phi$ in Eq. (2) exemplifies the experimental Al'tshuler-Aronov-Spivak (AAS) oscillation. Thus, the quantity A (including its sign) is closely related to the amplitude of the experimental AAS oscillation ($h/2e$), where R_{xx} is measured as a function of B. Letting $k_\pm=k_x\pm ik_y$ [$k_\nu\equiv -i(\partial/\partial\nu)$, where $\nu=x$, y or z], the Rashba (H_R) and Dresselhaus (H_D) hamiltonians for (001) oriented III-V semiconductor quantum well are given as [5]

$$H_{\mathrm{R}} = \alpha\left(k_y\sigma_x - k_x\sigma_y\right) = \begin{pmatrix} 0 & i\alpha k_- \\ -i\alpha k_- & 0 \end{pmatrix}, \text{ and} \tag{3}$$

$$H_{\mathrm{D}} = \mathrm{b}_{41}^{6c6c} \begin{pmatrix} 0 & \frac{1}{4}k_-\left(k_+^2 - k_-^2\right) - k_+\left\langle k_z^2\right\rangle \\ \frac{1}{4}k_+\left(k_-^2 - k_+^2\right) - k_-\left\langle k_z^2\right\rangle & 0 \end{pmatrix}, \tag{4}$$

respectively, where $\langle\ \rangle$ means the expectation value calculated using the confined wave function along the z axis. The total Hamiltonian $H_{\mathrm{S.O.}}$=H_{R}+H_{D} has the following structure: $H_{\mathrm{S.O.}} = \begin{pmatrix} 0 & h_{\mathrm{S.O.}} \\ h_{\mathrm{S.O.}}^* & 0 \end{pmatrix}$, where $h_{\mathrm{S.O.}}{}^*$ is the complex conjugate of $h_{\mathrm{S.O.}}$. We note that $H_{\mathrm{S.O.}}$ is the most general S.O. Hamiltonian including both the Rashba and Dresselhaus effects of all orders. Now, let us consider the time evolution of a spin state for an electron with an in-plane wave vector $\mathbf{k}$=(k_x, k_y), *i.e.*, $\Psi(t) = e^{-i\frac{H_{\mathrm{S.O.}}}{\hbar}t}\Psi_i(0)$. Converting t to L (length) using $L \equiv v_{\mathrm{F}}t = \frac{\hbar k_{\mathrm{F}}}{m^*}t$, where m^* is the effective mass (m^*=0.047m_e) for the conduction electrons, we perform the series expansion on $e^{-i\frac{H_{\mathrm{S.O.}}}{\hbar}\frac{m^*L}{\hbar k_{\mathrm{F}}}}$, which can be considered as the spin rotation operator. Letting $\tilde{h} \equiv \frac{m^*L}{\hbar^2 k_{\mathrm{F}}}h_{\mathrm{S.O.}}$,

$$\begin{aligned} e^{-i\frac{H_{\mathrm{S.O.}}}{\hbar}\frac{m^*L}{\hbar k_{\mathrm{F}}}} &= \mathbf{I} - i\begin{pmatrix} 0 & \tilde{h} \\ \tilde{h}^* & 0 \end{pmatrix} - \frac{1}{2!}\begin{pmatrix} 0 & \tilde{h} \\ \tilde{h}^* & 0 \end{pmatrix}^2 + \frac{i}{3!}\begin{pmatrix} 0 & \tilde{h} \\ \tilde{h}^* & 0 \end{pmatrix}^3 + \cdots \\ &\equiv \cos(\theta/2)\,\mathbf{I} - i\sin(\theta/2)\begin{pmatrix} 0 & e^{-i\psi} \\ e^{i\psi} & 0 \end{pmatrix} = \begin{pmatrix} \cos(\theta/2) & -ie^{-i\psi}\sin(\theta/2) \\ -ie^{i\psi}\sin(\theta/2) & \cos(\theta/2) \end{pmatrix}, \end{aligned} \tag{5}$$

where $\mathbf{I}$ is the identity matrix. Here, we also defined $\theta/2 \equiv |\tilde{h}|$ and $e^{-i\psi} \equiv \tilde{h}/|\tilde{h}|$. Thus, we see that Eq. (5) denotes a spin rotation by a angle θ about the axis $\hat{\zeta}$≡(cosϕ, sinϕ, 0), employing the right-handed screw rule.

In analyzing the experimental results, a special attention should be paid to the definition of the crystallographic indices. We define the indices following the convention used in the semiconductor industry [6]. In this convention, group III and V atoms are, respectively, placed at (0, 0, 0) and (1/4, 1/4, 1/4), or the equivalent sites, in zinc-blend structure. Then, $\hat{x}$, $\hat{y}$ and $\hat{z}$ directions in H_{R} and H_{D} [Eqs. (3) and (4)] are in the [0$\bar{1}$0], [100] and [001] directions, respectively. We note that such correspondences differ from the more natural $\hat{x}$|| [100], $\hat{y}$ || [010] and $\hat{z}$ || [001], which are the cases if group V and group III atoms are, respectively, placed at (0, 0, 0) and (1/4, 1/4, 1/4), or the equivalent sites. The latter choice is generally used by in the field of $\mathbf{k}\cdot\mathbf{p}$ theory and *ab initio* calculations [7]. For clarity, the indices following the latter convention are also shown in Fig. 1(a) with the subscript "th" such as $[100]_{\mathrm{th}}$.

With these in mind, one can obtain the analytic form of the SI amplitude $A(\theta_{\mathrm{D}}, \theta_{\mathrm{R}})$ as follows.

$$A(\theta_{\mathrm{D}},\theta_{\mathrm{R}}) = \left(\frac{[\mathbf{R}_{\mathrm{TOT}}]_{11} + [\mathbf{R}_{\mathrm{TOT}}]_{22}}{2}\right)^2 - \frac{1}{2} = \frac{1}{4}\left\{1 + 2\cos\theta_{\mathrm{D}}\cos\theta_{\mathrm{R}} - \cos(\theta_{\mathrm{D}} - \theta_{\mathrm{R}})\cos(\theta_{\mathrm{D}} + \theta_{\mathrm{R}})\right\}^2 - \frac{1}{2}, \tag{6}$$

where θ_{D}=$\frac{2m^*}{\hbar^2}(\beta L - \alpha\Delta L)$ and θ_{R}= $\frac{2m^*}{\hbar^2}(\alpha L - \beta\Delta L)$. Shown in Fig. 1(b) is three-dimensional plot of $A(\theta_{\mathrm{D}}, \theta_{\mathrm{R}})$.

3. Comparison with the experimental results

Shown in Fig. 2(g)-(i) are the experimental TRAC curves (-$\delta g_0^{\mathrm{AAS}}$ vs. N_{S}) measured at 300 mK for devices with L=1.8 μm and ΔL= -0.4, 0.0 and 0.4 μm, respectively, together with the results of our extended SI model [Fig. 2(a)-(c)], where the amplitude of the AAS h/2e oscillation in the electric conductance per loop is extracted by FFT and denoted as $\delta g_0^{\mathrm{AAS}}$. We also note that these devices were fabricated using sample1 wafer in Ref. 8. The reminiscent of the WAL effect, which manifests itself in the negative background of TRAC curves, is visible in these devices for all N_{S}s. The details of this effect will be discussed elsewhere [9]. Another feature found in the TRAC curves is the "*wiggling*". We marked dip- and peak-like features in the TRAC curves in Fig.2(g)-(i). We note that these features are highly reproducible. For example, the positions and the amplitudes of the "*wiggling*" repeated among devices that have identical structures and were prepared on a same epi-wafer, but at different times (typically more than a year apart). A noteworthy result is the fact that period of the appearance of the dip and peak features in the TRAC curves depended on the ΔL value of the pertinent structure. In this respect, we plotted, in Fig. 2(d)-(f), the wiggling part of the TRAC curves, denoted as $\delta g_{0,\,\mathrm{wiggle}}^{\mathrm{AAS}}$, subtracting the negative background, shown by the red lines in Fig. 2(g)-(i), from the TRAC curves somewhat arbitrarily. We found the period of the wiggling features increases with increasing ΔL, though such tendency is less obvious between devices with ΔL=0.0 and 0.4 μm. The explanation of

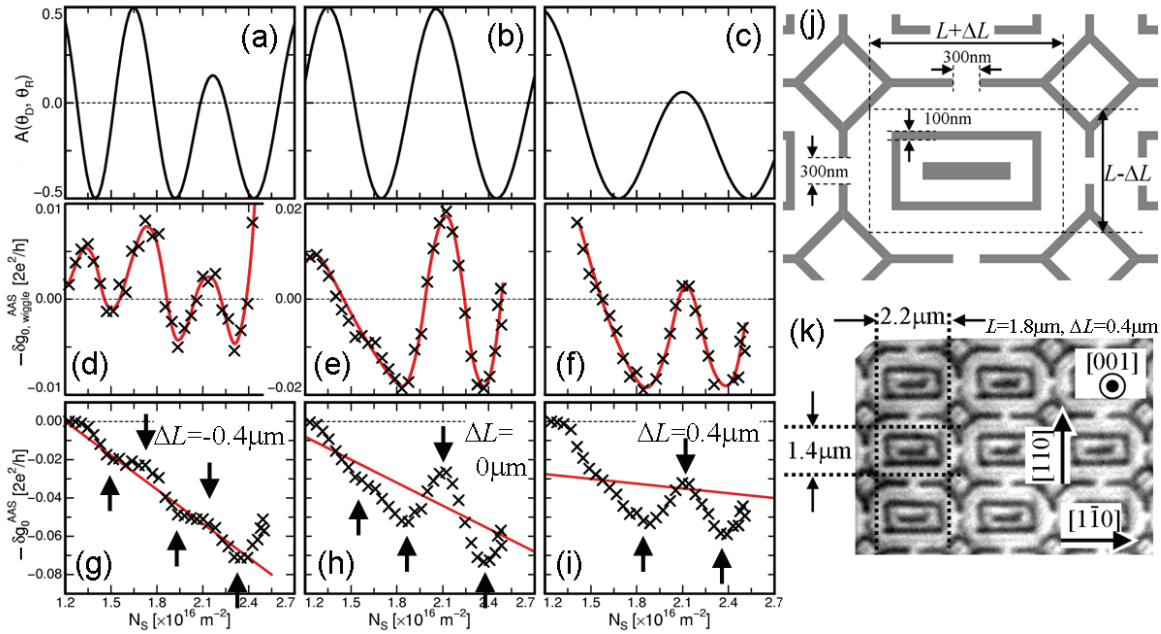

Fig. 2. (a)-(c) Plots of $A(\theta_D, \theta_R)$ for L=1.8 μm and ΔL = -0.4, 0.0 and 0.4 μm, respectively. The other parameters used in the calculation include the interaction parameter E_p=22eV [8] and b_{41}^{6c6c}= 27eVÅ^3 in Eq. (4). N_1=3.65, 3.85 and 4.10×10^{24}m^{-3}, and d_{QW}=9.6, 9.4 and 8.8 nm were used in (a), (b) and (c), respectively. (d)-(f) The "*wiggling*" part of the AAS amplitudes vs. N_S (TRAC curves), subtracting the background components shown by the red lines from the $-\delta g_0^{AAS}$ vs. N_S data, both shown in (g)-(i), for the devices with ΔL = -0.4, 0.0 and 0.4 μm, respectively. The red curves in (d)-(f) are guides to the eyes. In (d)-(i), the values in ordinate were negated to make their signs match those of $A(\theta_D, \theta_R)$. (j) Detailed design of the fabricated structure. (k) UV micrograph of the sample with ΔL = 0.4 μm. The darker region represents the etched part of the sample and the lighter reagion represents the unetched part where the conduction electrons reside. The electric current was passed in the [110] direction in all samples.

the latter feature may require more sophisticated model than our SI model. We note that the positions and amplitudes of the simulated dips and peaks varied sensitively with the doping density N_1 below the QW [8] and the QW thickness d_{QW}. Nevertheless, the periods of their appearance were less sensitive to N_1 and d_{QW}. We also note that we confirmed the information on the crystallographic indices of our samples that was provided by the wafer supplier by the facet observation at the wet-etched line and space structures [9,10].

Based on all the information provided above, we conclude that the crystallographic anisotropy of the S.O. interaction predicted from H_R and H_D [Eqs. (3) and (4)] has been confirmed successfully in the present experiment.

References

[1] T. Koga, J. Nitta, and M. van Veenhuizen, Phys. Rev. B **70**, 161302(R) (2004).
[2] T. Koga, Y. Sekine, and J. Nitta, Phys. Rev. B **74**, 041302(R) (2006).
[3] G. Engels, J. Lange, Th. Schäpers, and H. Lüth, Phys. Rev. **B 55**, R1958 (1997).
[4] T. Bergsten, T. Kobayashi, Y. Sekine and J. Nitta, Phys. Rev. Lett **97**, 196803 (2006).
[5] R. Winkler, *Spin-Orbit Coupling Effects in Two-Dimensional Electron and Hole Systems*, Springer-Verlag, Berlin Heidelberg, (2003).
[6] H. C. Gatos and Mary C. Lavine, J. Electrochem. Soc. **107**, 427 (1960).
[7] H. Riechert and S.F. Alvarado, Phys. Rev. Letters **52**, 2297 (1984); M. Cardona, N. E. Christensen, M. Dobrowolska, J. K. Furdyna and S. Rodriguez, Solid State Commun. **60**, 17 (1986); M. Cardona, N. E. Christensen, and G. Fasol, Phys. Rev. B **38**, 1806 (1988)
[8] T. Koga, J. Nitta, T. Akazaki, and H. Takayanagi, Phys. Rev. Lett. **89**, 046801 (2002).
[9] S. Faniel, T. Koga, S. Mineshige, T. Matsuura, and Y. Sekine, unpublished (2009).
[10] S. Adachi and H. Kawaguchi, J. Electrochem. Soc. **128**, 1342 (1981).